International Journal of Innovative Research and Scientific Studies, 8(6) 2025, pages: 157-179

IJIRSS
International Journal of Innovative Research & Scientific Studies

ISSN: 2617-6548

URL: www.ijirss.com

Adaptive mobilenetv3 with spatial attention-aided effective brain tumor classification approach using denoised image-based segmentation

Kulkarni Sheetal Vijay[1*], S. Poornapushpakala[2]

[1,2]Department of Electronics and Communication Engineering Sathyabama Institute of Science & Technology Chennai 600119, Tamilnadu, India.
[1]Department of Instrumentation Engineering AISSMS Institute of Information Technology Pune 411001, Maharashtra, India.

Corresponding author: Kulkarni Sheetal Vijay (*Email: sheetal.kulkarni@aissmsioit.org*)

Abstract

The collected images are processed through an image denoising module, where the Sparse Autoencoder (SAE) is employed for denoising images. The denoised images are then used in the brain tumor segmentation module, utilizing Cascaded MobileUnet++ (CMUnet++) for accurate localization of tumor regions. The segmented images are subsequently fed into the Adaptive MobileNetV3 with Spatial Attention (AMSA) for classification performance. Parameters from MobileNetV3 are optimized using Modified Random Integer-based Fossa Optimization (MRI-FO) to design an AMSA model for brain tumor classification with high accuracy. The inclusion of Spatial Attention (SA) helps the model prioritize relevant features in the segmented images. This model maintains stable performance even when tumors are subtle or difficult to detect. The accuracy of the MRI-FO-AMSA approach exceeds that of 72% CNN, 89% SVM, 86% VGG-16, and 86% AMSA. The proposed technique enhances brain tumor detection by effectively analyzing complex and irregular tumor shapes with high accuracy. This approach has the potential to improve brain tumor diagnosis accuracy, leading to better patient outcomes through timely and precise treatment.

Keywords: Adaptive MobilenetV3 with Spatial Attention, Brain Tumor Segmentation and Classification, Image Denoising; Cascaded MobileUnet, Modified Random Integer-based Fossa Optimization.

DOI: 10.53894/ijirss.v8i6.9515
Funding: This study received no specific financial support.
History: Received: 25 June 2025 / **Revised:** 29 July 2025 / **Accepted:** 31 July 2025 / **Published:** 27 August 2025

Competing Interests: The authors declare that they have no competing interests.
Authors' Contributions: Both authors contributed equally to the conception and design of the study. Both authors have read and agreed to the published version of the manuscript.
Transparency: The authors confirm that the manuscript is an honest, accurate, and transparent account of the study; that no vital features of the study have been omitted; and that any discrepancies from the study as planned have been explained. This study followed all ethical practices during writing.
Publisher: Innovative Research Publishing

1. Introduction

Brain tumors are caused by the abnormal growth in the brain and it can damage the nervous system [1]. One of the less dangerous brain tumor types is benign, and the patients affected by this type of tumor have a higher survival rate. The malignant tumors are highly dangerous, and their ability to spread faster reduces the chances of survival [2]. In order to protect neurons in the brain, glial cells are present in the brain, and they are affected by glioma tumors. Meningiomas are another common form of brain tumor, and they form in the protective layers of tissues in the brain [3]. Pituitary tumors develop at the base of the brain and affect the pituitary gland. Identifying the tumor type and its location is vital for an accurate diagnosis process to ensure the best treatment options based on the tumor type [4].

X-ray imaging uses electromagnetic waves to showcase fractured bones, while computed tomography (CT) scans visualize detailed views of internal body parts [5]. Among these techniques, MRI is considered the most effective imaging modality for examining nervous tissues [6]. MRI images help to identify brain tumors and assist radiologists in providing treatments based on the patient's condition. Radiologists have two approaches for diagnosing brain tumors, which include categorizing MRI scans to identify tumour types and distinguishing between normal brain MRI images [7]. Brain MRI is a vital neuroimaging tool used to detect deviations from normal brain activity that are useful for diagnosing and monitoring brain tumors [8]. MRI scans are used to detect, characterize, and monitor the growth of tumors for appropriate treatment planning. Furthermore, these images offer details regarding the brain's soft tissue that are beneficial in understanding both structural and functional assessments of the brain [9]. During the collection of MRIs, external and environmental conditions lead to the introduction of noise in brain MRI images [10]. This issue leads to information loss as it affects the crucial features needed for the detection process. Therefore, there is a high probability of misdiagnosis due to the loss of incomprehensible details [11].

Convolutional Neural Networks (CNNs) have gained more attention from researchers due to their performance in disease detection tasks [12]. CNN models excel in visual image processing, and they do not require additional preprocessing procedures [13]. CNNs enhance accuracy and feature extraction by offering improved performance in categorizing brain tumor types and grades compared to existing machine learning methods [14]. The advancements in machine learning and computer vision models are useful in performing tasks such as detection, classification, as well as segmentation. However, many existing Computer-Aided Diagnosis (CAD)-aided detection models that use CNNs face challenges in attaining efficient results and require more computational resources to perform well [15]. Lighter CNN models are not capable of precisely locating the tumor, as they require an additional segmentation process to identify the exact regions of the tumor. However, the computational demands of most conventional segmentation techniques are high [16]. Moreover, most of the models are not compatible in handling large volumes of images, and they often result in slower performance and suboptimal results [17]. Therefore, a deep learning-aided mechanism for brain tumor identification is introduced in this paper.

- To propose a deep learning-assisted brain tumor recognition method for offering treatments based on the identified cases to improve the survival rate. The model ensures efficient localization of tumor regions with an accurate image-denoising process that is useful for attaining precise classification outcomes. The robustness of the suggested technique is high due to its ability to process and refine images for analyzing the tumor regions.
- To introduce SAE for image denoising to remove unwanted noise while preserving the important features in brain images. The ability of the SAE model to perform unsupervised learning helps to remove noise in input images without losing key features. This process results in cleaner images for obtaining better outcomes in brain tumor detection procedures. It minimizes false positive results caused by unwanted noise in images.
- To employ the CMUnet++ model for precise tumor segmentation for the detection of tumor regions by accurate localization. This technique has the potential to handle tumors with different shapes and sizes. CMUnet++ is a cascaded architecture that is beneficial in refining segmentation outcomes. This leads to segmenting tumors that are even present at the borders of the brain.
- To design an AMSA for brain tumor classification to determine cases with high accuracy. The inclusion of SA helps the model prioritize relevant features in the segmented image. The performance of this model is stable, even if the tumors are subtle or difficult to detect. Moreover, it detects tumors with irregular shapes for accurate classification.
- To optimize the parameters of MobileNetV3, an MRI-FO algorithm is introduced that increases the effectiveness of tumor classification by fine-tuning the model's parameters with high robustness. MRI-FO enhances both the performance and the computational speed of the AMSA. This optimization ensures that the developed AMSA model can handle more datasets in less time while classifying tumor cases.

The layout of this paper is organized as follows: In sub-division II, the details of conventional techniques utilized for detecting brain tumors are provided. The fundamental illustrations of the developed technique with its explanation, are presented in sub-division III. The image denoising and segmentation tasks are discussed in Subdivision IV. In sub-division V, the brain tumor classification approach is described. The simulation findings are presented in sub-division VI, and the conclusion is given in sub-division VII.

2. Literature Survey

2.1. Related Works

Asiri et al. [18] have presented a two-module computational technique to improve the precision of identifying brain tumors. The authors addressed some problems such as fluctuating low region contrast and noise in the input by normalizing the images with image enhancement techniques. Then, the brain tumor recognition was performed using a machine learning technique. As per the experimental findings, the suggested model was effective in recognizing different kinds of brain tumors.

Khushi et al. [19] have employed EfficientNet models for recognizing brain tumors, as they are capable of identifying anomalies and performing feature extraction. A publicly accessible multiclass dataset was used in this study. Initially, the images were resized and cropped, and then noise was eliminated from the images. The EfficientNetB7 model achieved more accurate outcomes than other conventional models.

Vaiyapuri et al. [20] have recommended a classification model for brain tumors on MRIs using an ensemble learning model. They identified and categorized different brain tumor types. The quality of images was increased, and three deep learning models were used for feature extraction. Finally, the brain tumor was identified via an optimized Denoising Autoencoder (DAE) technique.

Almufareh et al. [21] have analyzed the performance of YOLOv5 and YOLOv7 in tumor detection. Three different types of tumors were identified and categorized in this work. Mask alignment mechanisms were used in the preprocessing step. The authors identified that both models were useful in precisely categorizing the tumors.

Juneja et al. [22] have performed image denoising on brain images using an autoencoder-based network. The researchers determined the performance of different denoising models with various measures. The proposed model provided noise-removed images in less time.

Balamurugan and Gnanamanoharan [23] have suggested a hybrid Deep CNN (DCNN) with an improved LuNet classifier for recognizing brain tumors. Preprocessing and segmentation were performed for precise results. The classification technique used features retrieved by the VGG16 model. The proposed model has lower computational complexity than conventional methods.

Khan et al. [24] have performed denoising and data augmentation on medical images using three different datasets. They used CNN to develop two deep learning algorithms for brain tumor diagnosis, and the suggested model attained better accuracy due to the incorporation of denoising techniques. The developed model was beneficial in the timely identification of brain tumors.

In Albalawi et al. [25] have performed using a single CNN model for recognizing brain tumors in MRI. The suggested CNN model attained high accuracy due to the utilization of optimization methods with feature extraction models. This model is helpful in treatment planning as it identifies the tumors in the early stages.

2.2. Problem Statement

The research on brain tumor detection using neuroimaging techniques has become increasingly important in recent years due to the life-threatening consequences of undiagnosed tumors. Accurate classification with deep learning is helpful in receiving the most effective treatment. High-quality medical images are essential for assisting doctors in detecting tumors. Conventional MRI denoising methods face several limitations, including information loss, degradation from compression, and difficulty in preserving essential edge features. Some of the obstacles faced by the existing techniques are listed below:

- Existing brain tumor detection models do not have the potential to deal with noisy or incomplete data. Even though some traditional methods perform denoising, they fail to preserve essential features in the input images while removing noise, which reduces the accuracy of tumor detection.
- Conventional tumor segmentation models, such as basic CNNs, have limitations in accurately locating tumor regions. These models lack the ability to analyze important regions of the brain, which impacts the overall accuracy of detection tasks.
- Many current classification models are not optimized for handling complex tumor variations. These models often rely on pre-determined parameters and fail to dynamically adjust to the unique characteristics of malignant and benign tumors, which affects the precision of classification performance.
- A significant issue with traditional brain tumor detection models is the high computational cost. Most deep learning architectures often require more computational resources.
- Most existing systems are not scalable to handle a large number of brain MRIs of patients. Conventional models struggle to maintain better performance across various tumour types and imaging conditions. Moreover, the use of complex segmentation techniques leads to inefficiencies in model performance that can delay the diagnosis process.

Several benefits and drawbacks of the prior brain tumor detection models are depicted in Table 1.

Table 1.
Benefits And Drawbacks Of The Prior Brain Tumor Detection Models.

Author [citation]	**Methodology**	**Features**	**Challenges**
Asiri et al. [18]	SVM	It enhances the image quality by improving the contrast and minimizing the noise in brain MRI images.	The generalizability of this technique is low.
Khushi et al. [19]	EfficientNet	This approach does not require more time and resources. This is highly adaptable to smaller datasets.	It needs to manage overfitting issues. It lacks efficient tumor region segmentation.
Vaiyapuri et al. [20]	DAE	It performs an advanced noise reduction process to retrieve useful features.	Its ability to analyze three-dimensional MRI is low.
Almufareh et al. [21]	YOLOv7	Accuracy is high due to the utilization of the mask alignment process. The technique allows simultaneous prediction of multiple bounding boxes quickly.	More computational resources are required while using larger datasets.
Juneja et al. [22]	BT-Autonet	It precisely visualizes the abnormal growth of tumours with the help of noise-free images.	Computational time is high.
Balamurugan and Gnanamanoharan [23]	DCNN	It obtains high accuracy in the segmentation process as it is capable of analyzing large volumes of images and recognizing tumors with different sizes and borders.	This approach is computationally complex and requires careful preprocessing to obtain accurate detection outcomes.
Khan et al. [24]	CNN	It has the ability to perform efficient tumour localization by enhancing the quality of images.	It results in less accuracy and needs longer computational times.
Albalawi et al. [25]	CNN	It precisely identifies the location of tumors in less time. Generalization capacity is high as it is efficient in handling diverse MRIs.	The model's interpretability is low. Analyzing the progression of the tumor is difficult.

3. Fundamental Illustration of Proposed Brain Tumor Classification Approach and its Dataset Description

3.1. Architecture of Developed Brain Tumor Classification Model

The primary goal of the proposed model is to efficiently segment and categorize brain tumors for treatment based on tumor type to increase survival rates. Collecting brain images from publicly available databases is the initial step. The images are then processed through an image-denoising module to remove unwanted noise without eliminating important features. This procedure is accomplished by the SAE model, and this approach is capable of handling unlabeled data as well as being beneficial in preserving important features. This denoising step is important as it ensures that the segmentation model receives clean and high-quality brain images, thereby reducing false positive results. The denoised images are fed into the brain tumor segmentation module, where CMUnet++ is employed to accurately segment tumor regions. This model can handle brain tumors of varying sizes and shapes. The segmentation step is useful for focusing only on the affected regions without analyzing unwanted background features. The use of CMUnet++ for segmentation helps manage memory and computational complexity issues. Next, the segmented images are shared with the AMSA mechanism for classification to differentiate normal from abnormal brain tumor cases. The AMSA model uses spatial attention mechanisms to focus on the most important features in the segmented image, which is useful for analyzing subtle tumor characteristics. The developed MRI-FO-AMSA is beneficial in classifying tumors with irregular shapes and accurately identifies subtle tumors due to the advantages of both MobileNetV3 and SA modules. The parameters of MobileNetV3 are optimized using the MRI-FO algorithm to improve its capability. The results of the implemented mechanism are validated against prior works to analyze its performance. The technical overview of the proposed brain tumor detection mechanism is shown in Figure 1.

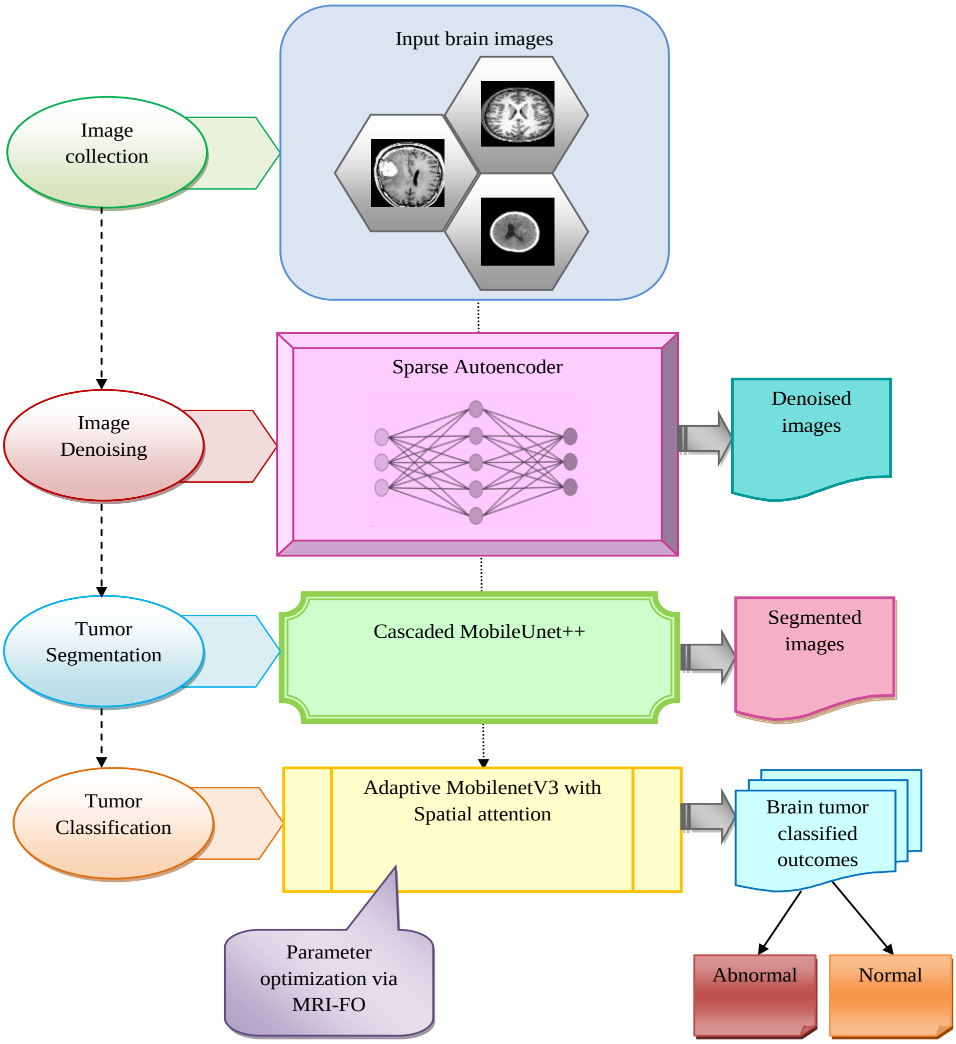

Figure 1.
Technical overview of the proposed brain tumor detection model.

3.2. Description of Brain Tumor Dataset

In this work, three different datasets are utilized to take brain MRI images. The descriptions are given below:

Dataset 1 (BRAMSIT): This dataset is accessed on 2025-02-15 from the source of https://sethu.ac.in/bramsit/. This dataset consists of brain MRIs of different age and with different genders. Along with normal and abnormal images, this dataset offers the ground truth of each image for efficient brain tumor detection.

Dataset 2 (youngp5/Yes-No-Brain-Tumor): This database is used to collect the brain MRIs and it is available on: https://huggingface.co/datasets/youngp5/Yes-No-Brain-Tumor. This dataset is accessed on: 2025-02-15. It contains two folders that indicate the presence and absence of tumors and each folder consists of 1500 images. It provides categorized files for performing training, testing, and validation.

Dataset 3 (JUH_MR-CT_dataset): This dataset is taken from https://data.mendeley.com/datasets/z4wc364g79/1 with an access date of 2025-02-15. 2D image slices are available on this database. Moreover, it offers both CT and MRI scans of the brain with high resolution.

The collected brain images are indicated as B_{MC} . The sample images from all these datasets are depicted in Figure 2.

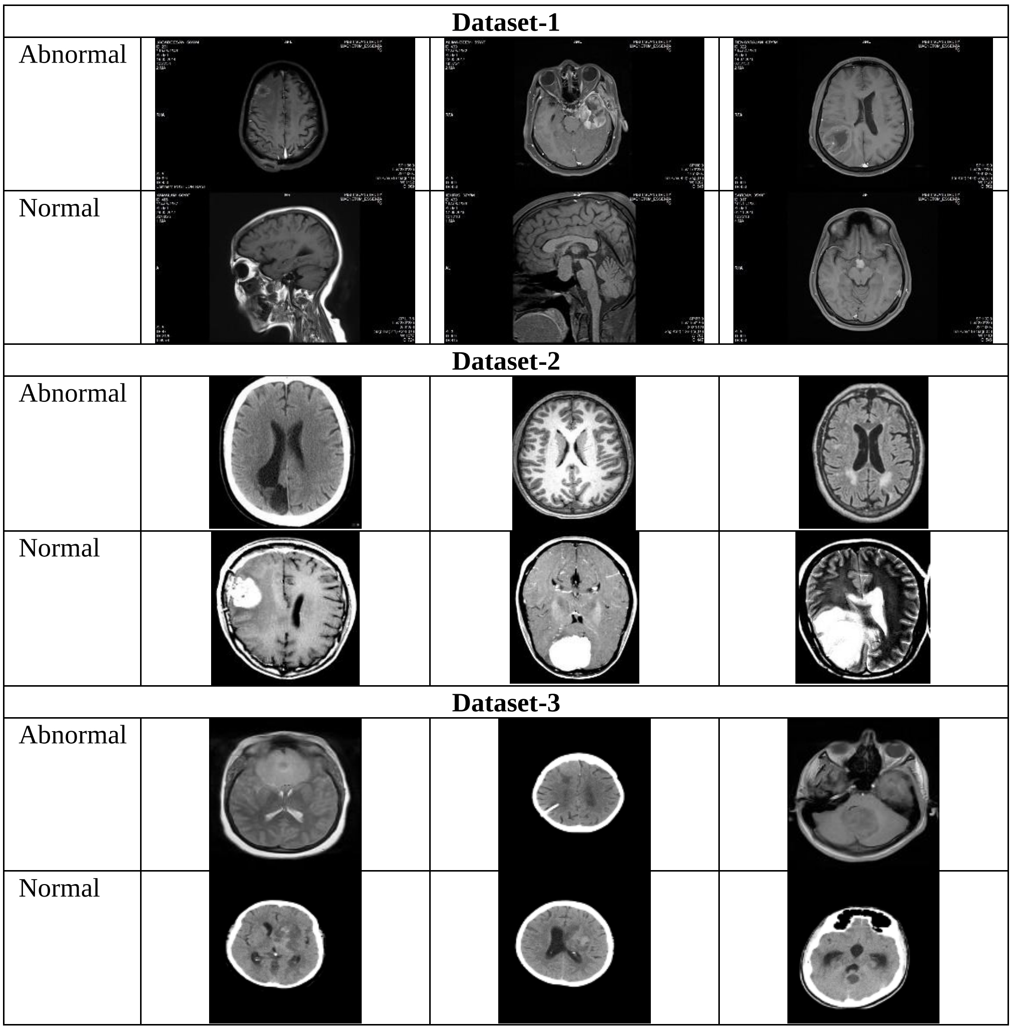

Figure 2.
Sample images from the brain image datasets.

4. Image Denoising-Based Cascaded Deep Learning Model for Segmentation of Brain Tumors

4.1. Sparse Autoencoder-based Image Denoising

The input images B_{MC} are denoised using the SAE [26] model for preserving the essential features in images by removing the unwanted noise. The inaccuracies during the segmentation process are avoided by eliminating the noise in input images with the help of the SAE model. More reliable and clean images are obtained from this model for further processing. Moreover, the loss of information problems are rectified by denoising the input brain images using the SAE model, as it preserves the essential tumor features.

The main aim of the SAE approach is to learn the representations of the input image. The sparsity function in this model is useful in reducing the reconstruction error. In this network, the utilization of sparsity is responsible for managing the use of neuron activations; if there are more activations, then a penalty function is activated. The average activation is handled by the sparsity proportion. Large weights are penalized to avoid overfitting issues by using L2 weight regularization in the SAE. The operation of SAE is mathematically derived in Equation 1.

$$\begin{aligned} B_{(n,h)} &= \frac{1}{2l}\Sigma_{p=1}^{l}\left\| s\left(Ny^{(p)}+p\right)-y^{(p)}\right\| \\ &+ \mu\Sigma_{q=1}^{m}\left(\rho\log^{\frac{\rho}{\hat{\rho}q}+(1-\rho)\log^{\frac{1-\rho}{1-\hat{\rho}q}}}\right) \\ &+ \frac{\alpha}{2}\Sigma_{r=1}^{R}\left\|N^{(r)}\right\|^{2} \end{aligned} \tag{1}$$

In the above equation, the strength of L2 weight regularization is mentioned as α . The sparsity weight and the sparsity proportion are indicated as μ and ρ , respectively. Input is referred as $y^{(p)}$. Activation function is given as $s(.)$. The variables h and n stands for bias and weight. The denoised images are specified by the term D_{mc}^{SAE} .

4.2. Mobile Unet++ Model

The Mobile Unet++ technique is utilized for brain tumour segmentation.

Mobile UNet++ [27] is an enhanced variant of the Mobile UNet architecture. The conventional UNet requires high computational resources, while the suggested model helps to maintain the accuracy of the segmentation process and minimize memory usage as well as processing complexity.

By using an encoder-decoder structure, the Mobile UNet++ model processes the denoised images by extracting the features. The depth-wise separable convolutions in this network split the spatial and channel-wise operations to reduce the computational overhead. Additionally, pointwise convolutions in this model enhance efficiency by reducing the number of feature channels. To improve stability, residual connections are incorporated into this network, preventing the gradient loss issue and enhancing segmentation performance.

The UNet++ architecture consists of additional intermediate convolutional blocks and skip connections that are presented between these blocks for obtaining semantically consistent outcomes. When compared to the basic MobileUnet model, the development of the MobileUnet++ technique simplifies the segmentation task with high accuracy. In the MobileUnet++ model, the semantic gap between the expanding and contracting blocks is connected by nested convolutional blocks $N^{a,b}$. The output of the convolution block is derived in Equation 2.

$$N^{a,b} = \begin{cases} CB\left(\left\langle N^{b-1,a} \right\rangle\right), & for\ a = 1 \\ CB\left(\left\langle \left\langle N^{b,p} \right\rangle_{p=1}^{a-1}, N^{b+1,a-1} \right\rangle\right), & for\ a > 1 \end{cases} \tag{2}$$

Here, the concatenation operation of attributes is termed as $N^{b,p}$. The output of a convolution block is provided as $CB(n)$. The structural view of the MobileUnet++ model is visualized in Figure 3.

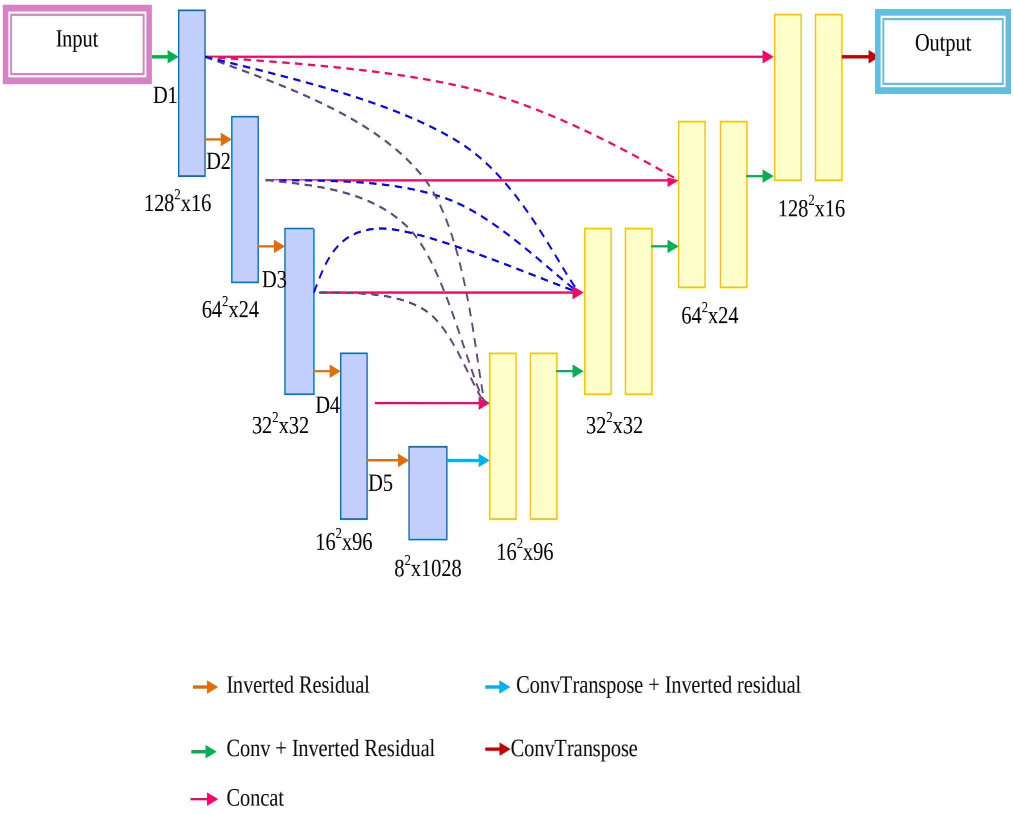

Figure 3.
Structural view of the MobileUnet++ model.

4.3. Segmentation using CMUNet++

The denoised images D_{mc}^{SAE} are segmented by the developed CMUNet++. CMUnet++ model enhances the performance of traditional MobileUNet architectures by employing a cascaded structure and replacing the UNet structure with UNet++ architecture. The encoder-decoder architecture of UNet++ is enhanced with skip connections that help to preserve the minute details in images. So, the tumor localization process does not eliminate the important features in the brain images. The proposed CMUnet++ model is cascaded, so it uses the segmented outputs from the previous layer to improve the segmentation accuracy. This cascading mechanism is useful in handling more complex and small tumor shapes. The UNet++ model focuses on high-level contextual information while segmenting brain tumors. This ability is essential in handling tumors presented in irregular boundaries. The integration of MobileNet in the architecture enhances the overall computational efficiency as MobileNet does not require additional parameters. Thus, the segmentation quality is improved and the computational load is decreased. The cascaded structure improves the segmentation of complex tumor shapes by refining the outcomes from previous layers. The use of skip connections and the cascaded design is useful in tackling complex tumor shapes effectively, as some of the tumors are in heterogeneous structures and they are often difficult to segment. Overall, the proposed segmentation model preserves the subtle tumor features and results in higher-quality segmented outcomes R_p^{Seg}. The schematic view of the CMUNet++-driven segmentation is shown in Figure 4.

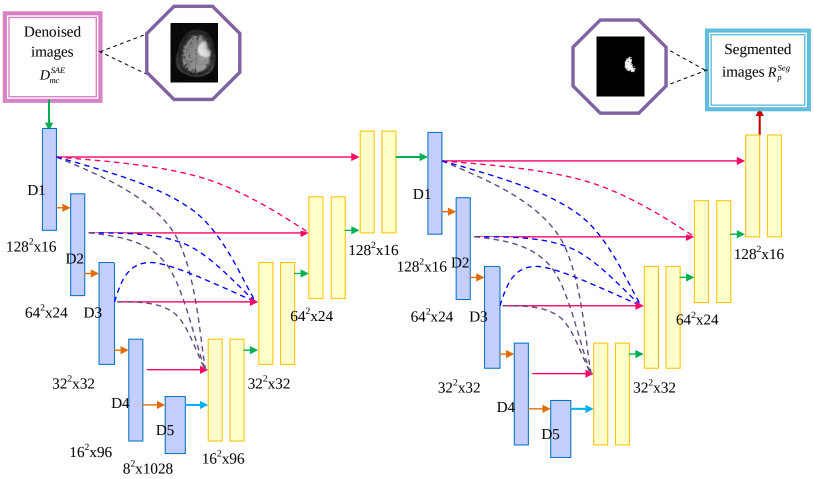

Figure 4.
Schematic view of CMUNet++-driven segmentation.

5. Categorization of Brain Tumor Types using an Adaptive Deep Learning Model

5.1. Description of MobileNetV3 Model

The MobileNetV3 [28] is used for brain tumor classification. The key feature of this model is the use of depthwise separable convolutions. This convolution is utilized to divide the standard convolution operations into pointwise processing and per-channel filtering. This decomposition process is useful to reduce the number of parameters and minimize computational complexity. In MobileNetV3, a convolution kernel is employed to simplify the feature extraction process. Additionally, bottleneck blocks have been refined with a lower expansion ratio of 4, which helps to decrease the count of intermediate channels. Then, the reduction ratio is increased to 16 for enhancing the performance of the Squeeze-and-Excitation (SE) block. This modification process reduces the computational overhead while improving the recalibration of channel-wise feature maps. Incorporating the SE into MobileNetV3 enhances the model's ability to focus on key characteristics while disregarding irrelevant features. This module is responsible for performing channel reweighting and global average pooling. This dynamic adjustment of weights allows the model to effectively extract important information. To further minimize memory usage, the dense layer is reduced to 128 neurons in the MobileNetV3 model. The diagram of MobileNetV3 is depicted in Figure 5.

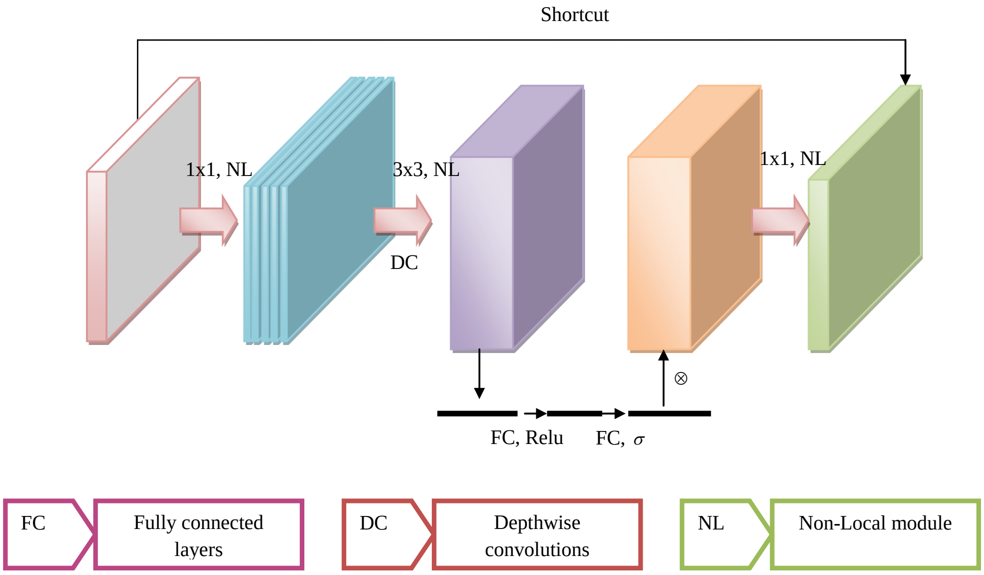

Figure 5.
Diagram of MobileNetV3.

5.2. Brain Tumor Classification using AMSA

The brain tumor classification is accomplished using the AMSA model that recognizes the abnormal and normal cases by using the segmented brain images R_p^{Seg} . The developed AMSA is an integrated version of the MobileNetV3 architecture with an SA mechanism that is useful for analyzing relevant features of the tumor. The SA mechanism helps to dynamically adjust its priority on important regions of the segmented image. This is beneficial for analyzing tumor-related features while not emphasizing irrelevant background information.

One of the variant of convolutional attention module is SA [29] and it is utilized for the classification task in this work. A feature descriptor is formed in this network by concatenating the average and max pooling operations. The channel-wise map pooling and average pooling receives the same input $S \in F^{X \times Y \times Z}$, then two

outputs $S_{Max}^k \in F^{X \times Y \times Z1}$ and $S_{Avg}^k \in F^{X \times Y \times Z1}$ are generated from both of the operations. Then, a spatial attention map $A^k(S) \in F^{X \times Y \times Z1}$ is produced by a feature descriptor module and this module uses a sigmoid function that is employed after the convolution layer. The output feature is computed based on Equation 3.

$$\begin{aligned} S^k &= S.A^k(S) \\ &= S.\sigma\left(s^{7\times7}\left(\left[Maxpool(S); Avergepool(S)\right]\right)\right) \\ &= S.\sigma\left(s^{7\times7}\left(\left[S_{Max}^k; S_{Avg}^k\right]\right)\right) \end{aligned} \tag{3}$$

Here, the sigmoid function is shown as $\sigma(.)$ and the convolution operation is denoted as $s^{7\times7}$.

The MRI-FO-AMSA model's capability to detect subtle differences between the tumors is enhanced by the combination of MobileNetV3 and the SA mechanism. The MobileNetV3 serves as the backbone of this network, and it is useful for handling the computational complexity issues. By analyzing the specific features in each image and focusing on the regions that visualize the presence of brain tumors, the AMSA obtains highly accurate classification results. The performance enhancement of the classification process is achieved through parameter optimization of MobileNetV3 using the MRI-FO algorithm. The objective function of the implemented brain tumor classification using MRI-FO-AMSA is given in Equation 4.

$$W = \underset{\left\{CE_N^{MV3}, ER_B^{MV3}, YU_G^{MV3}\right\}}{\arg\min} \left(\frac{1}{Accuracy} + \frac{1}{\Pr ecision} + FNR \right) \tag{4}$$

Here, the number of epochs tuned in the range of $[5-50]$ is stated as YU_G^{MV3}. The hidden neuron count and the learning rate are specified as ER_B^{MV3} and CE_N^{MV3}, both are optimized in the range of $[5-255]$ and $[0.01-0.99]$, respectively. The calculations of the precision, False Negative Rate (FNR) and accuracy is expressed in Equations 5-7.

$$precision = \frac{N^{tp}}{N^{tp} + M^{fp}} \tag{5}$$

$$FNR = \frac{M^{fn}}{N^{tp} + M^{fn}} \tag{6}$$

$$Accuracy = \frac{N^{tp} + N^{tn}}{N^{tp} + N^{tn} + M^{fp} + M^{fn}} \tag{7}$$

The terms M^{fn} , N^{tp} , M^{fp} and N^{tn} stands for false negative, true positive, false positive and true negative. The illustrative diagram of MRI-FO-AMSA-assisted brain tumor classification is shown in Figure 6.

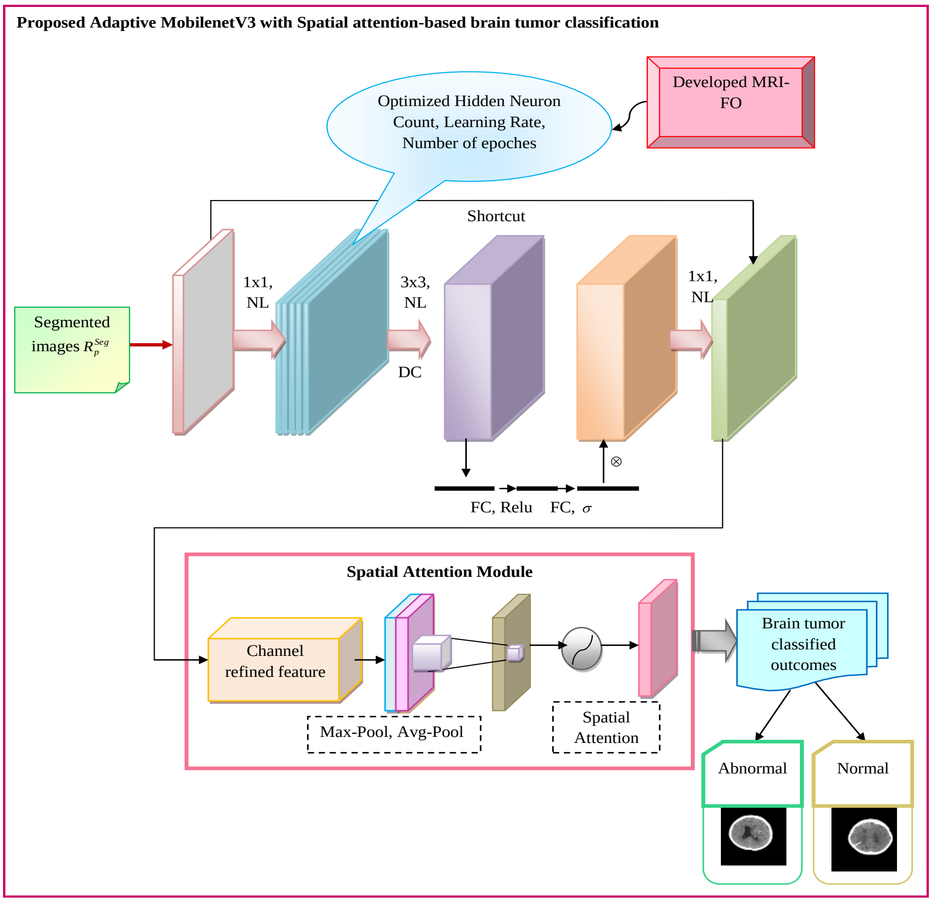

Figure 6.
Illustrative diagram of brain tumor classification using MRI-FO-AMSA.

5.3. Solution Encoding using MRI-FO

The optimization process is essential in this proposed work to enhance the efficacy of the classification model. Therefore, an MRI-FO algorithm is developed to fine-tune the parameters of MobileNetV3. This optimization aids in accurately distinguishing between normal and abnormal cases. Optimizing the parameters of MobileNetV3 improves the generalization capacity of the presented classification model. Consequently, the optimal parameter configuration maximizes the classification effectiveness and robustness in brain tumor detection. The conventional FOA [30] is designed based on the hunting strategies of the fossa. Based on the attack and positional change of the fossa, the exploration and exploitation phases are developed, resulting in better optimization outcomes. Moreover, this algorithm is useful for both binary and multi-objective problems. However, the chances of converging to local optima in complex landscapes are high. Depending on the population size, the FOA requires more computation time and resources. Therefore, the concept of FOA is improved by modifying its random attribute, which helps to overcome the persistent issues in FOA. In MRI-FO, the random attribute j is expressed in Equation 8.

$$j = \frac{BD}{CD} - PD \times \frac{1}{BD - PD} \tag{8}$$

Here, the variables PD, BD and CD denotes the best fitness, worst fitness, and current fitness. The best solution is obtained based on the evaluation of the highest fitness values. The MRI-FO explores all the areas by modifying the random attribute based on the fitness functions mentioned in the above expression. So, the proposed MRI-FO quickly converges toward optimal solutions without being affected by local optima issues like conventional FOA. Furthermore, the optimal performance of the MRI-FO is maintained throughout all the iterations even if the population size increases. The pseudocode of the MRI-FO is visualized in Algorithm 1.

Algorithm 1: Implemented MRI-FO
Input: Initial parameter of the classification model
Allocate the population size K
Set the total number of iterations C
While termination condition not met
    Arrange the solution space in a random manner
        For $i = 1:\mathrm{C}$
            Compute the fitness of all fossa
            Update the random attribute j as given in Equation 8
            Based on the behaviour of fossa determines its movement

Update the location of fossa
End for
End while
Find best solution
Output: Fine-tuned parameters from the MobileNetv3

6. Performance Analysis and Discussions

6.1. Simulation Configuration

The implementation of the presented work was carried out using Python. The population size was initialized as 10 during the implementation, while the total number of iterations and chromosome length were set to 50 and 3, respectively. The performance analysis of the designed model was conducted among existing techniques such as CNN [24], SVM [18], and VGG-16 [19]. Also, algorithms such as Archimedes Optimization Algorithm (AOA) [31], Mine Blast Optimization (MBO) [32], Black Widow Optimization (BWO) [33] and FOA [30] were considered. Segmentation techniques like Unet [34], ResUnet [35] and MobileUnet [27] were used to validate the performance of tumor localization.

6.2. Evaluation Metrics

The efficiency of the MRI-FO-AMSA model is evaluated by considering various evaluation criteria. The segmentation performance is validated by considering Intersection over Union (IoU) as well as Peak Signal-to-Noise Ratio (PSNR) measures. Classification performance is estimated by considering several positive and negative measures including accuracy and False Positive Rate (FPR). The computations of FPR, Dice coefficient, IoU, and PSNR measures utilized for performance assessment are shown in Equations 9-12.

$$\mathrm{F}PR = \frac{M^{fp}}{M^{fp} + N^{tn}} \tag{9}$$

$$Dice\,Coefficient = \frac{2N^{tp}}{2N^{tp} + M^{fn} + M^{fp}} \tag{10}$$

$$IoU = \frac{N^{tp}}{N^{tp} + M^{fp} + M^{fn}} \tag{11}$$

$$PSNR = 10\log_{10}\left(\frac{Max_P^2}{MSE}\right) \tag{12}$$

Here, the maximum value of a pixel is signified as Max_P^2.

6.3. Segmentation Results

The denoised and segmented brain tumor images are depicted in Figure 7.

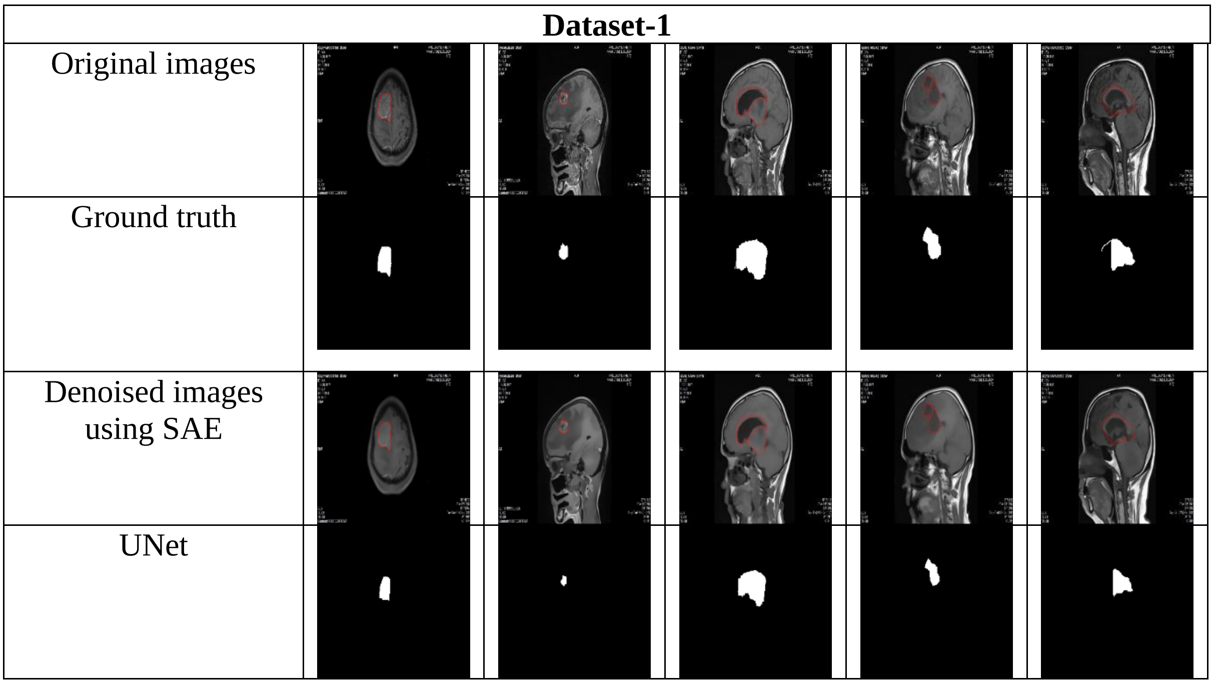

ResUnet	
MobileNet	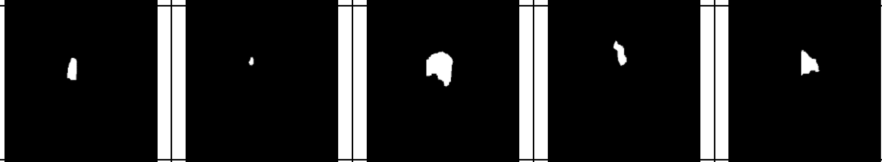
Suggested CMUnet++	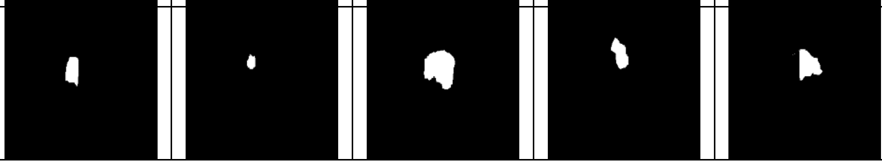
Dataset-2	
Original images	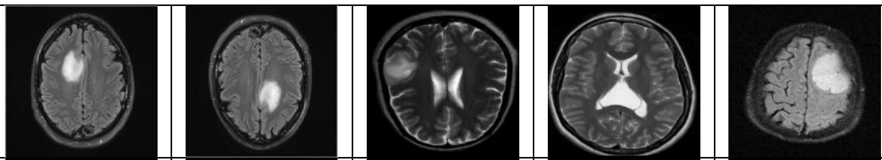
Ground truth	
Denoised images using SAE	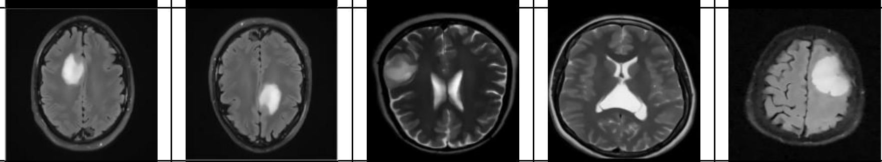
UNet	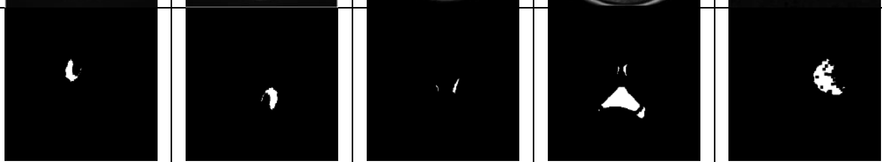
ResUnet	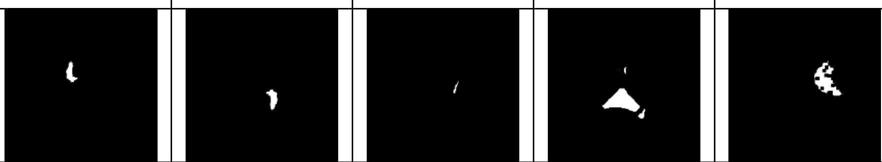
MobileNet	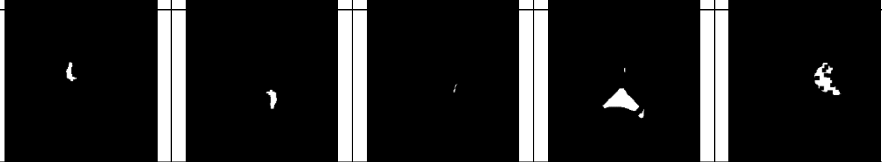
Suggested CMUnet++	
Dataset-3	
Original images	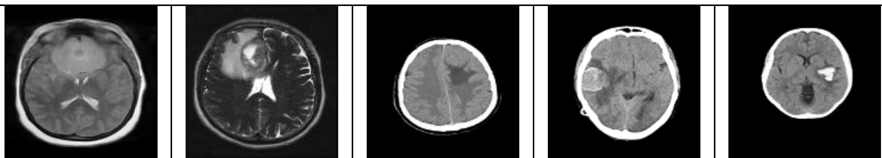

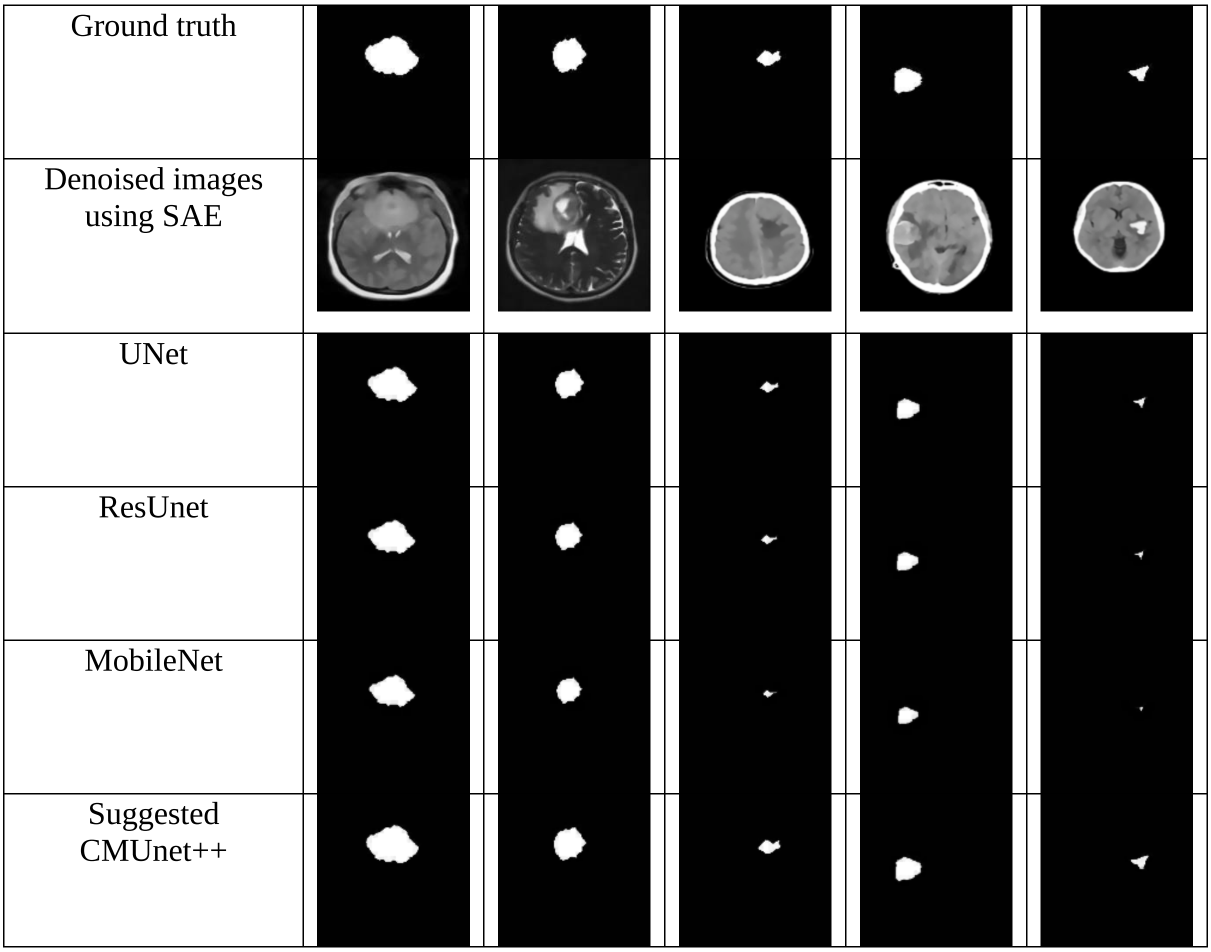

Figure 7.
Segmented brain tumor images using CMUnet++.

6.4. Performance Analysis of Denoising Process

The accuracy of the denoising process done on the collected brain images using the SAE model for further detection process is analyzed and the results are illustrated in Figure 8 indicates the performance of the developed SAE among varying noises in the images. The Structural Similarity Index (SSIM) of the recommended model is higher in removing noise such as salt-and-pepper, Poisson noise, Gaussian noise, and speckle noise in the images via the SAE technique for all three datasets. The quality of the images is not reduced after noise removal, as confirmed by the improved PSNR and SSIM results. This demonstrates that the utilized SAE module accurately denoises brain images while learning the representations of the input image without any information loss.

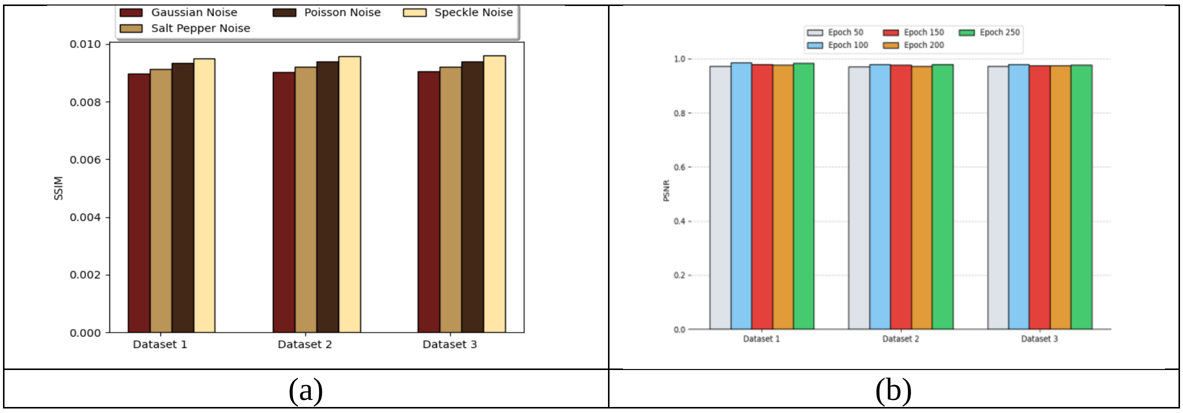

Figure 8.
Performance Analysis of Brain Image Denoising Process by Varying a) SSIM and b) PSNR.

6.5. Analysis of Brain Tumor Segmentation Performance

The segmentation results in Figure 9 indicate that the proposed CMUnet++ achieves the highest IoU score, which proves the capability of the implied segmentation approach. The improved segmentation performance of the proposed CMUnet++ is attained by a cascaded architecture, as it helps with better feature refinement and multi-scale representation. The results show that Unet and ResUnet obtained lower accuracy and IoU values, as they are not capable of accurate feature tuning, while MobileUnet and MUnet++ performed better, but the proposed CMUnet++ model outperformed all the models. The superior IoU score of CMUnet++ proves its capability to accurately capture tumor boundaries by reducing segmentation errors. Moreover, the high accuracy result of the developed model justifies that it has the potential to handle complex tumor structures more effectively.

Dataset-1

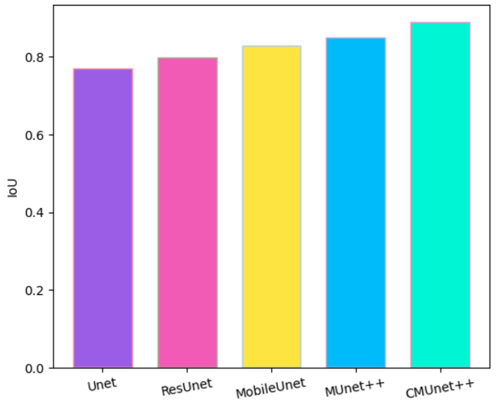

(a)

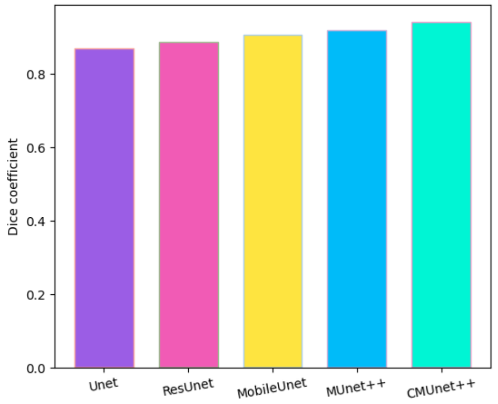

(b)

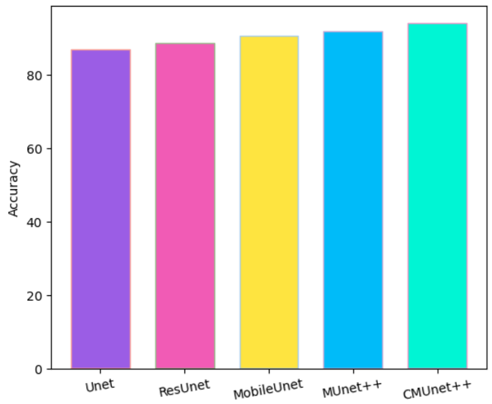

(c)

Dataset-2

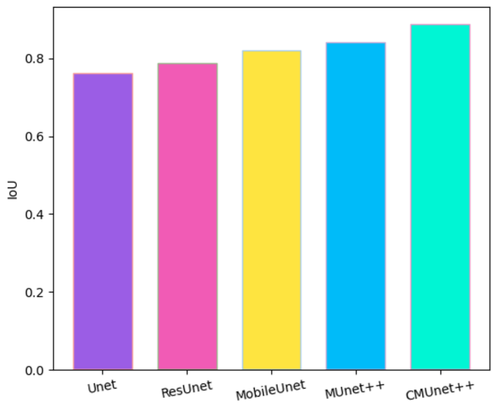

(a)

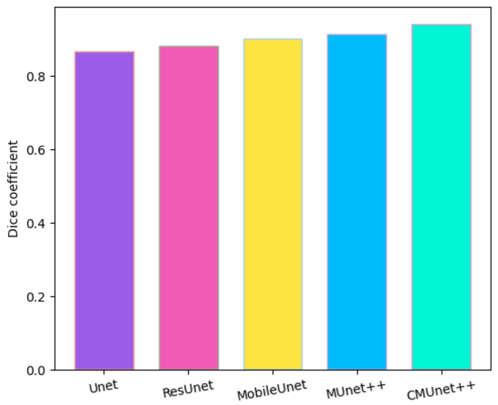

(b)

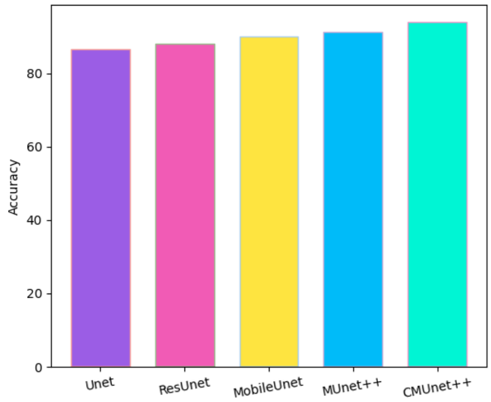

(c)

Dataset-3

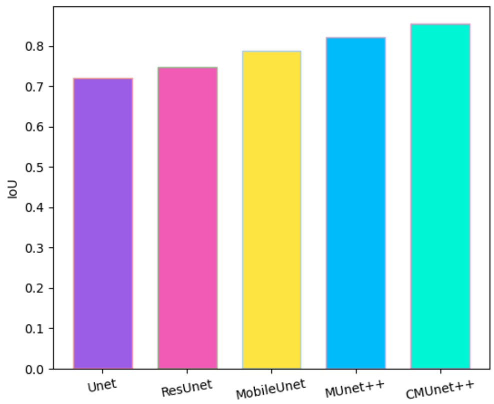

(a)

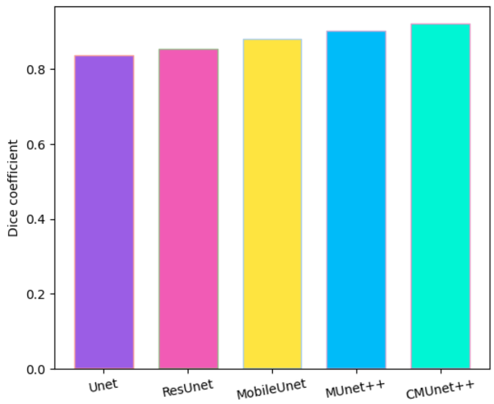

(b)

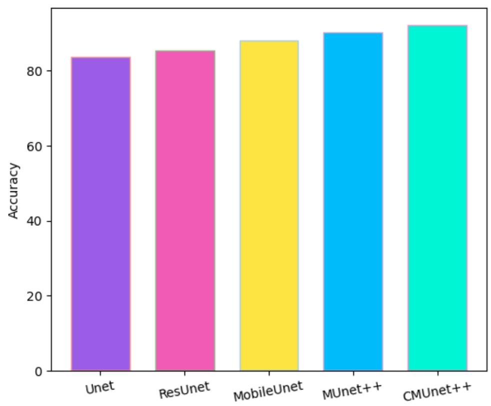

(c)

Figure 9.
Analysis of Brain Tumor Segmentation Performance with Respect to a) IoU, b) Dice coefficient, and c) Accuracy.

6.6. Assessment of Brain Tumor Classification Performance

The classification performance of the proposed MRI-FO-AMSA model is depicted in Figure 10 and Figure 11. The suggested model is evaluated against existing techniques, including CNN, SVM, VGG-16, MBO-AMSA, BWO-AMSA, AOA-AMSA, and FOA-AMSA. The accuracy of the MRI-FO-AMSA model at 500 epochs is 99%, 97%, and 94% for datasets 1, 2, and 3, respectively. The integration of MRI-FO with AMSA enhances the feature learning process on segmented images with optimal parameter tuning, resulting in improved classification outcomes, as shown in the results. For dataset 2, the precision of MRI-FO-AMSA is 96% at 100 epochs, while the precision achieved by MBO-AMSA, BWO-AMSA, AOA-AMSA, and FOA-AMSA is 79%, 86%, 86.1%, and 84%, respectively. The incorporation of the SA model with the MobileNetV3 technique has increased the accuracy of detecting specific characteristics within segmented regions. Although the proposed AMSA performs well, the use of MRI-FO further improves classification effectiveness compared to prior models.

Dataset-1

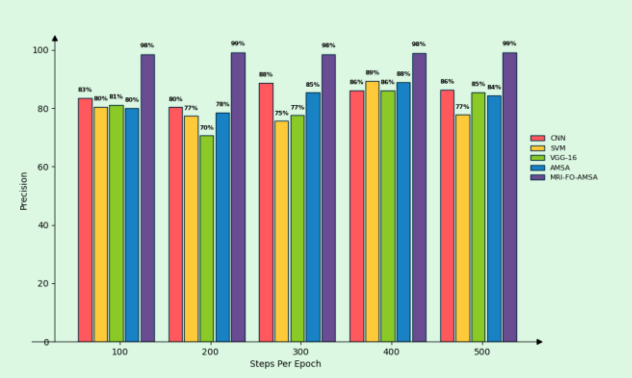

(a)

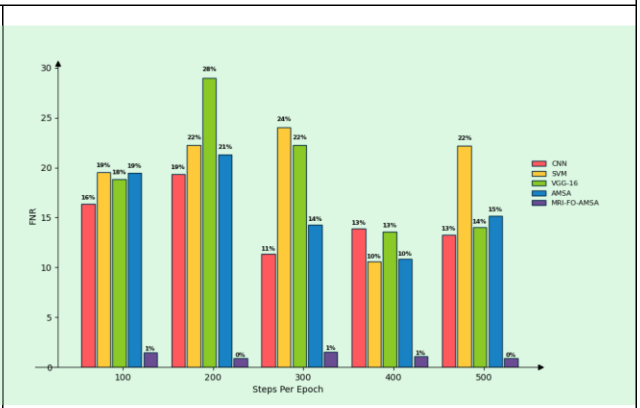

(b)

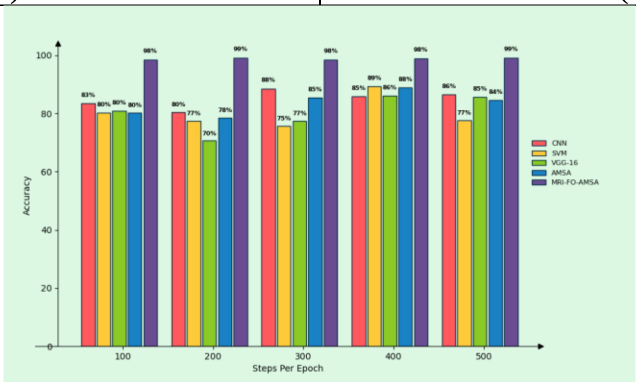

(c)

Dataset-2

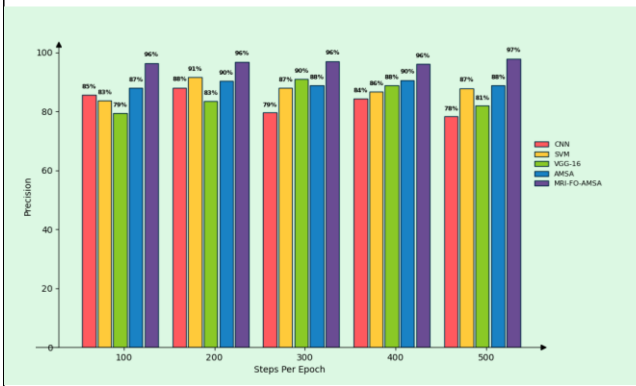

(a)

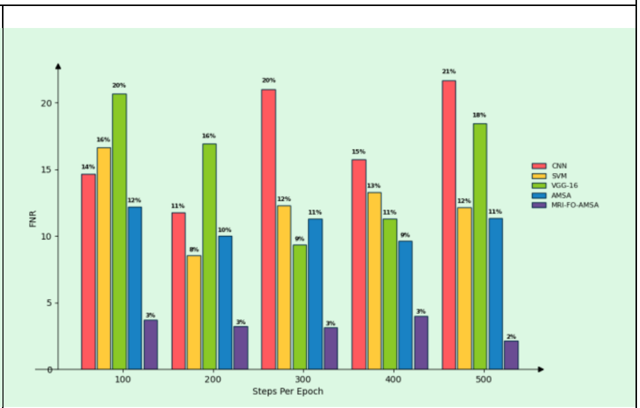

(b)

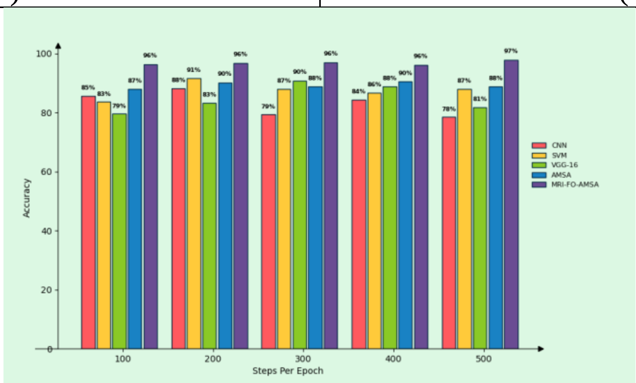

(c)

Dataset-3

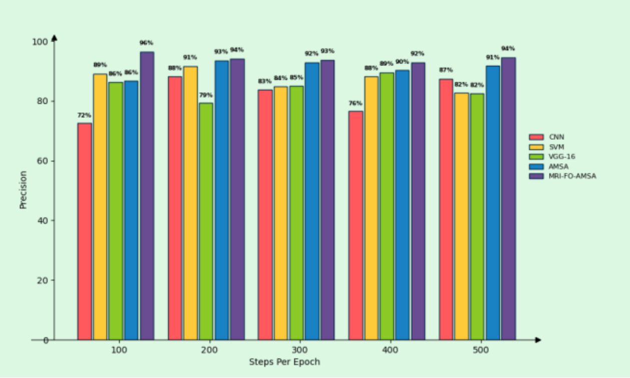

(a)

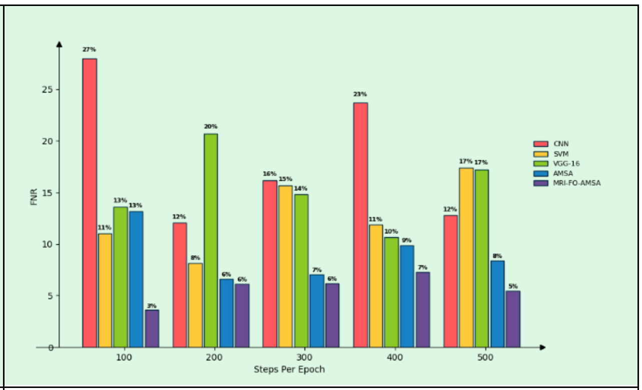

(b)

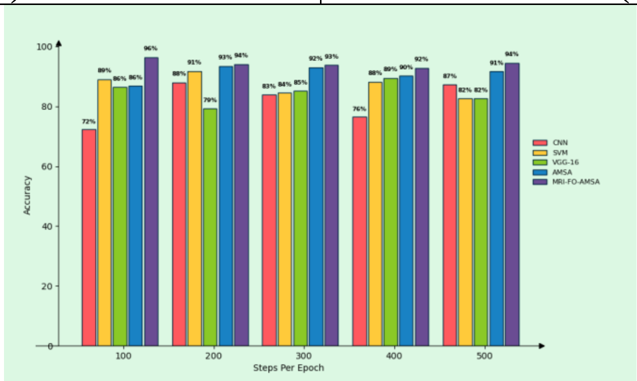

(c)

Figure 10.
Brain Tumor Categorization Performance Assessment over Existing Classifiers in Terms of a) Precision, b) FNR, and c) Accuracy.

Dataset-1

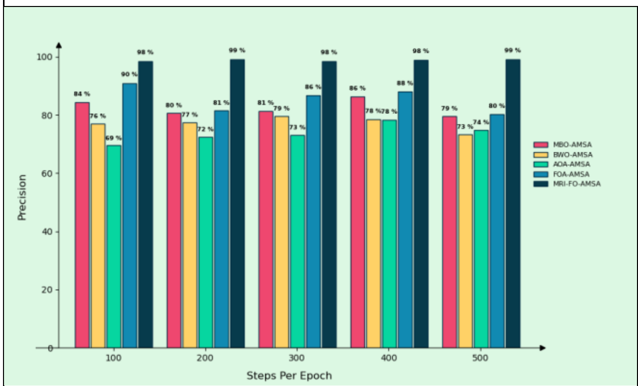

(a)

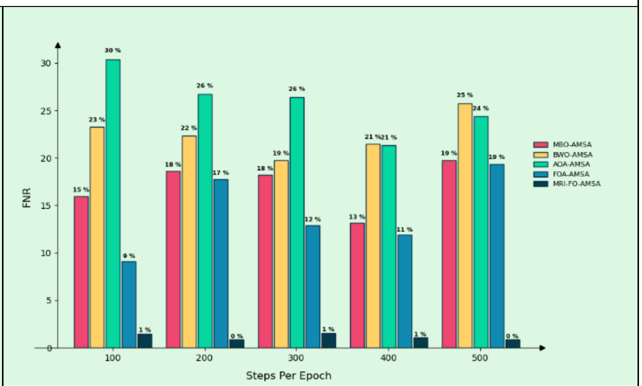

(b)

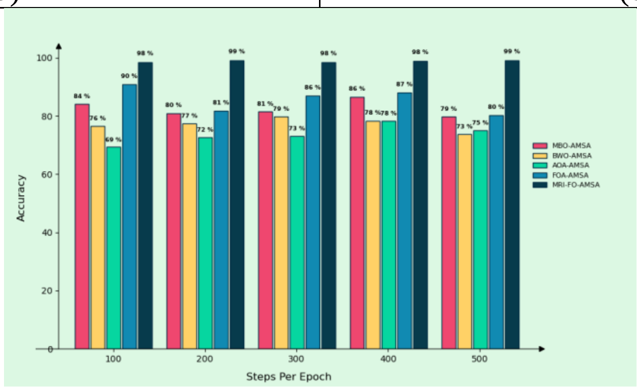

(c)

Dataset-2

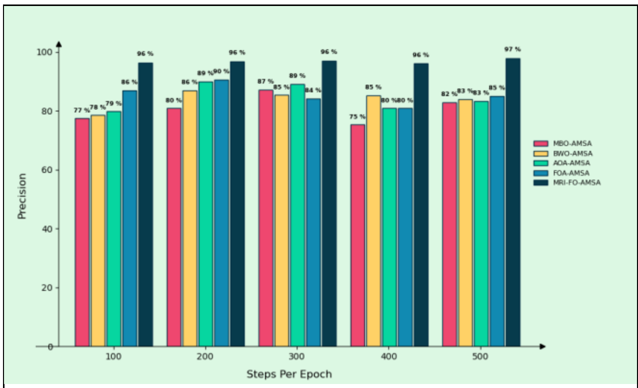

(a)

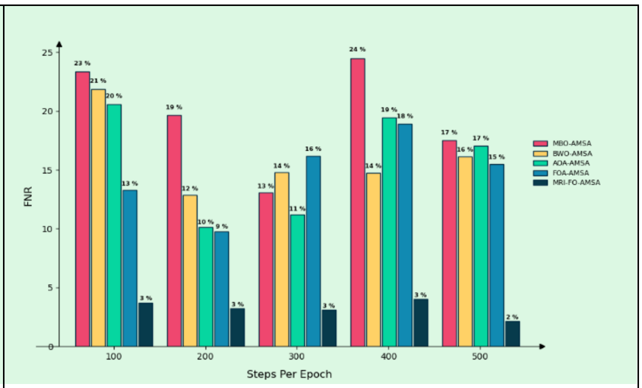

(b)

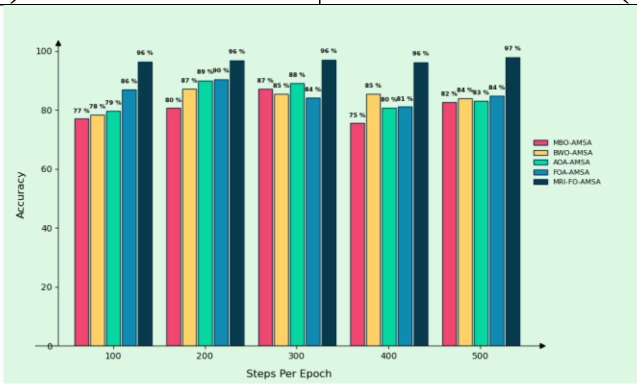

(c)

Dataset-3

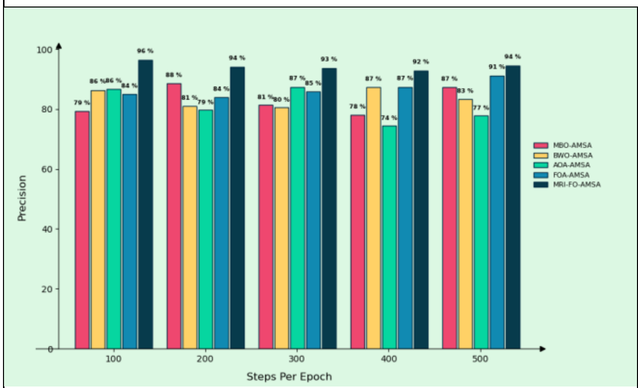

(a)

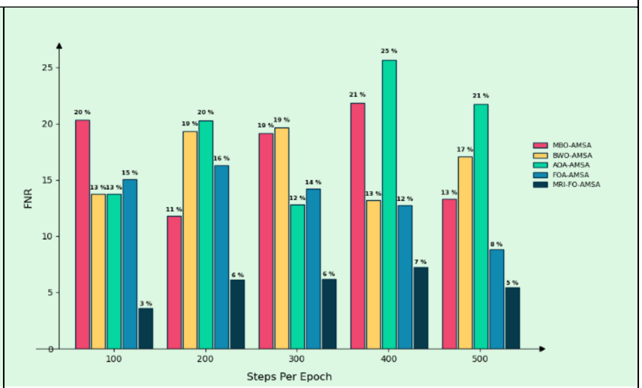

(b)

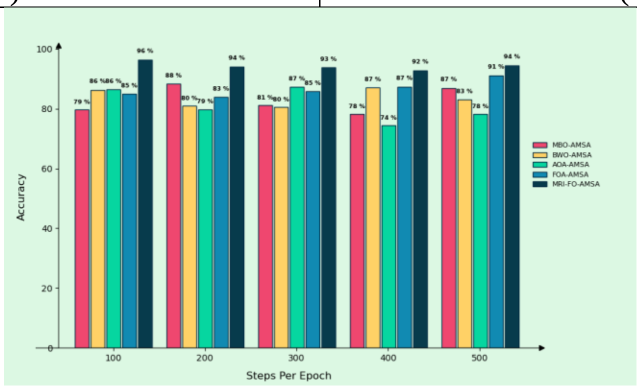

(c)

Figure 11.
Brain Tumor Categorization Performance Assessment Among Various Heuristic Algorithms in Terms of a) Precision, b) FNR, and c) Accuracy.

6.7. ROC and Convergence Analysis

The ROC curve and convergence evaluation of the MRI-FO-AMSA model is exhibited in Figure 12 and Figure 13. The MRI-FO-AMSA model achieves a better ROC curve than CNN, SVM, and VGG-16, demonstrating its superior capability in distinguishing between normal and abnormal cases. The optimized feature AMSA model enhances classification performance through the use of inverted residual blocks in its architecture, which accurately focus on the important characteristics needed for brain tumor classification in segmented images. The false positive rate of the traditional CNN model is higher than that of other models, indicating its poorer discrimination ability. These results show that the proposed MRI-FO-AMSA minimizes classification errors through parameter tuning in AMSA. The use of MRI-FO ensures that the parameters of MobileNetV3 are fine-tuned for optimal classification performance. The generalization of the derived method is also higher, as it produces consistent classification outcomes across three different databases.

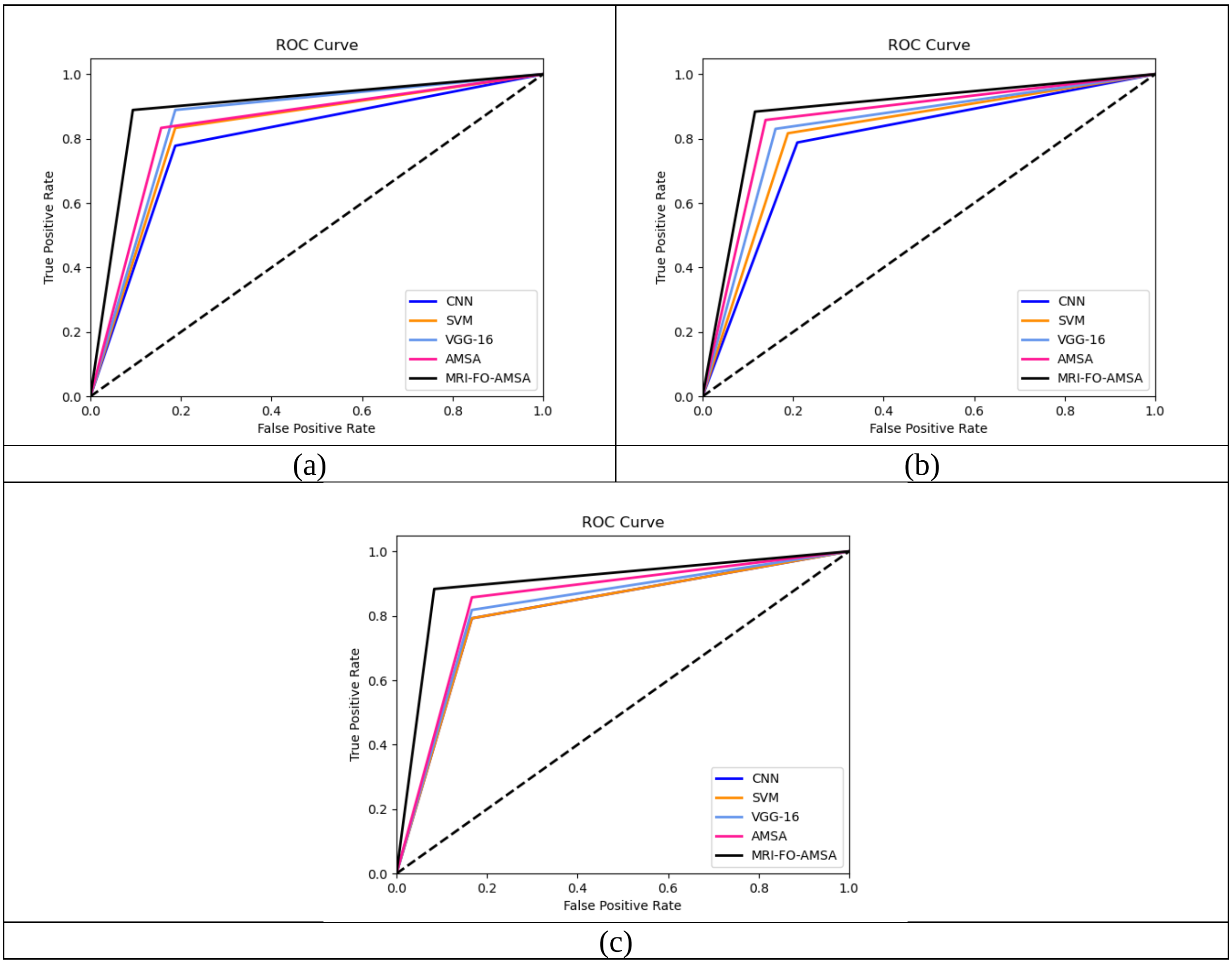

Figure 12.
ROC assessment of the proposed brain tumor detection model by means of a) Dataset 1, b) Dataset 2 and c) Dataset 3.

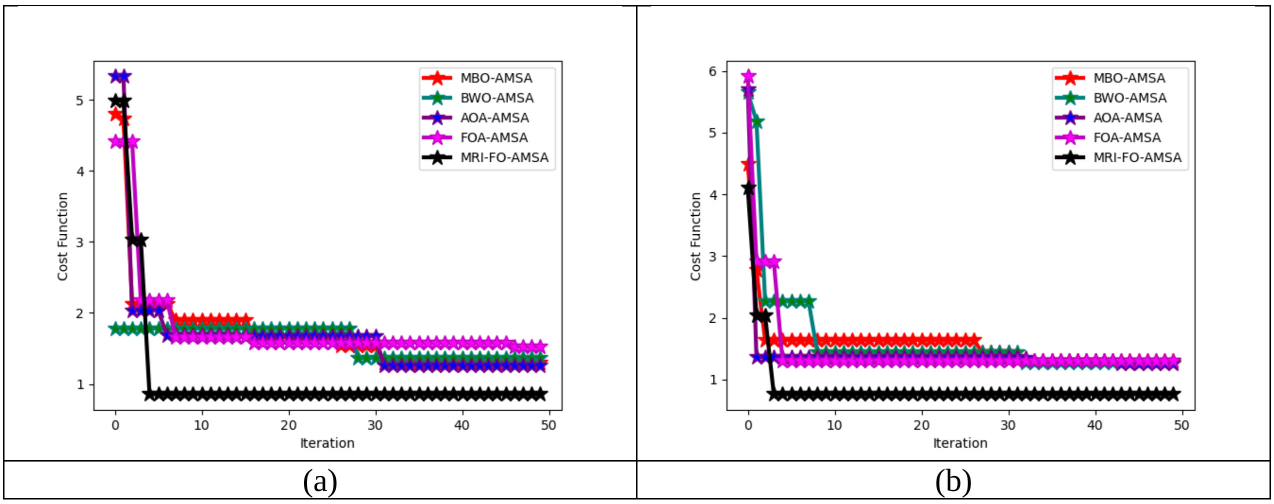

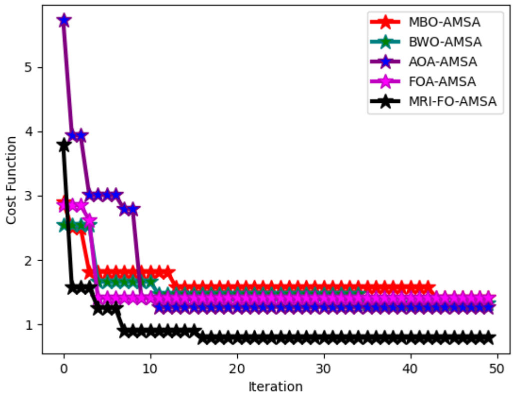

(c)

Figure 13.
Convergence assessment of the proposed brain tumor detection model by means of a) Dataset 1, b) Dataset 2 and c) Dataset 3**.**

6.8. Statistical Evaluation

The statistical evaluation outcomes of the MRI-FO-AMSA are depicted in Table 2. For Dataset 1, the executed model achieves the best result of 0.855614; for Dataset 2, the result is 0.761013; and for Dataset 3, it is 0.791568. These results confirm the stability of the introduced technique in accurately classifying brain tumor cases. Both the segmentation and classification processes performed by the proposed techniques outperform other models based on the mean and median scores of the presented model. For Dataset 3, the standard deviation score of the developed method is 0.456426, which confirms the potential of the proposed model in handling numerous brain images. The statistical results justify that the MRI-FO-AMSA model is reliable across multiple datasets, with a lower error rate due to the integration of advanced techniques. The combination of denoising, advanced segmentation, AMSA-based classification, and optimization with MRI-FO enhances performance in brain tumor detection.

Table 2.
Statistical Evaluation Of The Introduced Technique.

Algorithm Comparisons					
Measures	**MBO-AMSA** Naidu et al. [32]	**BWO-AMSA** Hayyolalam and Kazem [33]	**AOA-AMSA** Hashim et al. [31]	**FOA-AMSA** Tareq et al. [30]	**MRI-FO-AMSA**
Dataset-1					
MEDIAN	1.655421	1.781076	1.670812	1.58485	0.855614
MEAN	1.724197	1.59881	1.694907	1.811601	1.108117
STANDARD DEVIATION	0.68242	0.205624	0.780627	0.677072	0.899993
WORST	4.801323	1.781076	5.331746	4.414085	4.991515
BEST	1.299586	1.366835	1.263705	1.530835	0.855614
Dataset-2					
STANDARD DEVIATION	0.480217	0.828558	0.61248	0.738378	0.524026
MEAN	1.573497	1.642291	1.423003	1.490122	0.878812
WORST	4.487918	5.65134	5.702187	5.912449	4.105199
BEST	1.298698	1.275344	1.260145	1.301274	0.761013
MEDIAN	1.638842	1.446908	1.36219	1.301274	0.761013
Dataset-3					
STANDARD DEVIATION	0.276664	0.314334	0.924726	0.377067	0.456426
MEAN	1.667102	1.538591	1.673899	1.519711	0.945725
BEST	1.417701	1.320192	1.2727	1.408845	0.791568
MEDIAN	1.578624	1.471841	1.2727	1.408845	0.791568
WORST	2.903619	2.5397	5.723554	2.853492	3.792175

6.9. Overall Performance Assessment

The classification performance assessment is conducted and the results are provided in Tables 3 and 4. At a batch size of 4, the MRI-FO-AMSA achieves 98.3% accuracy, whereas only 88.96%, 89.7%, 85.16%, and 91.78% accuracy are attained by MBO-AMSA, BWO-AMSA, AOA-AMSA, and FOA-AMSA for dataset 1. Even if the batch size increases, the performance of AMSA improves due to the inclusion of MRI-FO-based optimization. When comparing all techniques, the CNN model's precision in classifying brain tumors is very low. This indicates that the combination of adaptive MobileNetV3 with SA techniques is effective for medical image classification, as it performed better than other conventional deep learning architectures. For dataset 2, the FPR of the CNN, SVM, VGG-16, and AMSA is 12.16%, 19.37%, 15.14%, and 10.78% at a batch size of 64. However, the proposed model significantly reduces misclassification results, attaining a very low FPR score of 1.42%. Therefore, the FPR scores of the implemented model demonstrate that the presented MRI-FO-AMSA handles images with varying sizes. Additionally, due to the denoising process, accurate segmentation is possible, resulting in fewer errors during classification.

Table 3.
Overall Performance Assessment Of The Proposed Model Against Other Algorithms.

Algorithm Comparisons					
Measures	**MBO-AMSA Naidu et al. [32]**	**BWO-AMSA Hayyolalam and Kazem [33]**	**AOA-AMSA Hashim et al. [31]**	**FOA-AMSA Tareq et al. [30]**	**MRI-FO-AMSA**
Dataset-1					
Median	1.655421	1.781076	1.670812	1.58485	0.855614
Mean	1.724197	1.59881	1.694907	1.811601	1.108117
Standard deviation	0.68242	0.205624	0.780627	0.677072	0.899993
Worst	4.801323	1.781076	5.331746	4.414085	4.991515
Best	1.299586	1.366835	1.263705	1.530835	0.855614
Dataset-2					
Standard deviation	0.480217	0.828558	0.61248	0.738378	0.524026
Mean	1.573497	1.642291	1.423003	1.490122	0.878812
Worst	4.487918	5.65134	5.702187	5.912449	4.105199
Best	1.298698	1.275344	1.260145	1.301274	0.761013
Median	1.638842	1.446908	1.36219	1.301274	0.761013
Dataset-3					
Standard deviation	0.276664	0.314334	0.924726	0.377067	0.456426
Mean	1.667102	1.538591	1.673899	1.519711	0.945725
Best	1.417701	1.320192	1.2727	1.408845	0.791568
Median	1.578624	1.471841	1.2727	1.408845	0.791568
Worst	2.903619	2.5397	5.723554	2.853492	3.792175

Table 4.
Overall Performance Assessment Of The Proposed Model Against Various Classifiers.

Algorithm Comparisons					
Batch size	**MBO-AMSA Naidu et al. [32]**	**BWO-AMSA Hayyolalam and Kazem [33]**	**AOA-AMSA Hashim et al. [31]**	**FOA-AMSA Tareq et al. [30]**	**MRI-FO-AMSA**
Accuracy					
Dataset-1					
4	88.96667	89.7	85.16667	91.78333	98.3
8	85.55	89.35	87.81667	93.65	99.13333
16	80.03333	87.41667	92.28333	94.16667	98.53333
32	90.26667	85.76667	89.23333	90.2	98.63333
64	86.43333	87.75	89.11667	92.86667	99.2
Dataset-2					
4	78.7	87.55	86.78333	87.51667	98.98333
8	85.21667	88.58333	84.06667	91.91667	98.7
16	86.33333	82.26667	87	92.16667	99.08333
32	76.68333	84.83333	86.2	92.66667	98.38333
64	79.25	88.66667	88.36667	93.55	98.61667
Dataset-3					
4	78.96667	86.46667	86.93333	86.41667	98.3
8	80.18333	86.46667	79.61667	86.83333	98.43333
16	82.23333	90.25	84.25	82.7	98.56667
32	71.23333	79.03333	78	89.26667	99.16667
64	85.2	91.5	83.66667	91.43333	98.9
FPR					

Dataset-1					
4	11.00399	10.32537	14.77046	8.097301	1.695479
8	14.28095	10.63476	12.16351	6.405576	0.864362
16	19.79306	12.48751	7.625708	5.817819	1.462766
32	9.626915	14.12392	10.79017	9.666667	1.363032
64	13.55482	12.20486	10.8674	7.085828	0.797872
Dataset-2					
4	21.9405	12.90213	13.82799	12.96108	1.054781
8	15.52941	11.80061	16.56545	8.381405	1.360544
16	14.02853	18.30176	13.37407	8.254398	0.952705
32	24.01216	15.58045	14.14004	7.60353	1.700102
64	21.56533	11.75474	12.05962	6.777364	1.429058
Dataset-3					
4	21.19601	13.57572	13.05945	13.61361	1.70227
8	19.87329	13.76908	20.45985	13.20881	1.568758
16	17.5957	9.749583	15.69087	17.4318	1.435247
32	28.81921	21.24421	22.12242	10.77385	0.834446
64	14.84323	8.511348	16.33267	8.715902	1.101469

7. Summary

A deep learning-driven model was introduced for performing brain tumor detection. The brain images were accumulated from publicly available databases. The images were then processed via the SAE module to remove any undesirable noise in the input images. The denoised images were used by CMUnet++ to accurately localize the tumor regions. The resultant images were utilized by the AMSA model for the classification task. To enhance the classification performance, the parameters of MobileNetV3 were optimized using the MRI-FO algorithm. The results of the established brain tumor detection model were validated against prior works to analyze its performance. At an epoch size of 100, for dataset 3, the accuracy of the MRI-FO-AMSA is 96%, meanwhile, the accuracy of techniques like CNN, SVM, VGG-16, and AMSA is 72%, 89%, 86%, and 86%. The proposed technique performed a better brain tumor detection process by analyzing complex and irregular tumor shapes with high accuracy. In the future, different types of brain tumors will be detected. Also, other pre-processing techniques for improving the contrast of the input images will be explored.

References

[1] M. Rasheed *et al.*, "Recognizing brain tumors using adaptive noise filtering and statistical features," *Diagnostics,* vol. 13, no. 8, p. 1451, 2023.

[2] J. Yan *et al.*, "Application of enhanced weighted least squares with dark background image fusion for inhomogeneity noise removal in brain tumor hyperspectral images," *Applied Sciences,* vol. 15, no. 1, p. 321, 2024.

[3] K. Ali, A. N. Qureshi, M. S. Bhatti, A. Sohail, M. Hijji, and A. Saeed, "De-noising brain mri images by mixing concatenation and residual learning (MCR)," *Computer Systems Science & Engineering,* vol. 45, no. 2, 2023.

[4] S. C. Prathipati and S. K. Satpathy, "A multilevel de-noising approach for precision edge-based fragmentation in MRI brain tumor segmentation," *Traitement du Signal,* vol. 40, no. 4, p. 1715, 2023.

[5] C. S. Alok, J. Singh, S. Kumar, N. Saxena, M. Gupta, and P. Verma, "Design and assessment of improved convolutional neural network based brain tumor segmentation and classification system," *Journal of Integrated Science and Technology,* vol. 12, no. 4, pp. 793-793, 2024.

[6] A. M. Samar *et al.*, "Improved brain tumor segmentation and classification in brain MRI with FCM-SVM: A diagnostic approach," *IEEE Access,* vol. 12, pp. 61312-61335, 2024.

[7] K. Shirin, M. Sabeti, M. H. Shakoor, and E. Moradi, "Deep multi-task learning structure for segmentation and classification of supratentorial brain tumors in MR images," *Interdisciplinary Neurosurgery,* vol. 36, p. 101931, 2024.

[8] A. Akter *et al.*, "Robust clinical applicable CNN and U-Net based algorithm for MRI classification and segmentation for brain tumor," *Expert Systems with Applications,* vol. 238, p. 122347, 2024.

[9] S. Deepa, J. Janet, S. Sumathi, and J. Ananth, "Hybrid optimization algorithm enabled deep learning approach brain tumor segmentation and classification using MRI," *Journal of Digital Imaging,* vol. 36, no. 3, pp. 847-868, 2023.

[10] D. Chandra Sekaran and J. Christopher Clement, "Enhancing brain tumor segmentation in MRI images using the IC-net algorithm framework," *Scientific Reports,* vol. 14, no. 1, p. 15660, 2024.

[11] M. S. Borse and T. R. Babu, "Accurate brain tumor image segmentation and classification using deep convolutional network (DCNN) and pulse coupled neural networks (PCNN)," *Frontiers in Biomedical Technologies,* 2024.

[12] G. Bompem and D. Pandluri, "Batch normalization based convolutional neural network for segmentation and classification of brain tumor MRI images," *International Journal of Intelligent Engineering & Systems,* vol. 17, no. 2, 2024.

[13] Z. M. Mirza *et al.*, "Brain tumor MRI classification using a novel deep residual and regional CNN," *Biomedicines,* vol. 12, no. 7, p. 1395, 2024.

[14] P. A. Babu *et al.*, "Optimized CNN-based brain tumor segmentation and classification using artificial bee colony and thresholding," *International Journal of Computers Communications & Control,* vol. 18, no. 1, 2023.

[15] A. Ilyasse, J. Riffi, K. el Fazazy, A. M. Mahraz, and H. Tairi, "3DUV-NetR+: A 3D hybrid semantic architecture using transformers for brain tumor segmentation with MultiModal MR images," *Results in Engineering,* vol. 21, p. 101892, 2024.

[16] B. Usharani, N. Chintalapudi, and G. Battineni, "Brain tumor detection and categorization with segmentation of improved unsupervised clustering approach and machine learning classifier," *Bioengineering,* vol. 11, no. 3, p. 266, 2024.

[17] D. Priyanka and R. Rohilla, "Brain tumor image pixel segmentation and detection using an aggregation of GAN models with vision transformer," *International Journal of Imaging Systems and Technology,* vol. 34, no. 1, p. e22979, 2024.

[18] A. A. Asiri, T. A. Soomro, A. A. Shah, G. Pogrebna, M. Irfan, and S. Alqahtani, "Optimized brain tumor detection: A dual-module approach for mri image enhancement and tumor classification," *IEEE Access,* vol. 12, pp. 42868-42887, 2024.

[19] H. M. T. Khushi, T. Masood, A. Jaffar, M. Rashid, and S. Akram, "Improved multiclass brain tumor detection via customized pretrained efficientnetb7 model," *IEEE Access,* vol. 11, pp. 117210-117230, 2023.

[20] T. Vaiyapuri, J. Mahalingam, S. Ahmad, H. A. Abdeljaber, E. Yang, and S.-Y. Jeong, "Ensemble learning driven computer-aided diagnosis model for brain tumor classification on magnetic resonance imaging," *IEEE Access,* vol. 11, pp. 91398-91406, 2023.

[21] M. F. Almufareh, M. Imran, A. Khan, M. Humayun, and M. Asim, "Automated brain tumor segmentation and classification in MRI using YOLO-based deep learning," *IEEE Access,* vol. 12, pp. 16189-16207, 2024.

[22] M. Juneja *et al.*, "Denoising of magnetic resonance images of brain tumor using BT-Autonet," *Biomedical Signal Processing and Control,* vol. 87, p. 105477, 2024.

[23] T. Balamurugan and E. Gnanamanoharan, "Brain tumor segmentation and classification using hybrid deep CNN with LuNetClassifier," *Neural Computing and Applications,* vol. 35, no. 6, pp. 4739-4753, 2023.

[24] M. F. Khan, A. Iftikhar, H. Anwar, and S. A. Ramay, "Brain tumor segmentation and classification using optimized deep learning," *Journal of Computing & Biomedical Informatics,* vol. 7, no. 01, pp. 632-640, 2024.

[25] E. Albalawi *et al.*, "Enhancing brain tumor classification in MRI scans with a multi-layer customized convolutional neural network approach," *Frontiers in Computational Neuroscience,* vol. 18, p. 1418546, 2024.

[26] Y. Li, J. Ren, Z. Gao, and G. Sun, "Sparse autoencoder based hyperspectral anomaly detection with the singular spectrum analysis based spectral denoising," in *Proceedings of the IGARSS 2024 - 2024 IEEE International Geoscience and Remote Sensing Symposium*, 2024.

[27] D. M. S. D. Rathlavath Kalavathi *et al.*, "Stratification of breast cancer images by utilizing spatial information and deep learning model," *Journal of Theoretical and Applied Information Technology,* vol. 102, no. 7, 2024.

[28] N. Sriwiboon and S. Phimphisan, "Efficient COVID-19 detection using optimized mobilenetv3-small with SRGAN for web application," *Engineering, Technology & Applied Science Research,* vol. 15, no. 2, pp. 20953-20958, 2025.

[29] C. Guo, M. Szemenyei, Y. Yi, W. Wang, B. Chen, and C. Fan, "Sa-unet: Spatial attention u-net for retinal vessel segmentation," in *2020 25th International Conference on Pattern Recognition (ICPR)*, pp. 1236-1242, 2021.

[30] H. Tareq *et al.*, "Fossa optimization algorithm: A new bio-inspired metaheuristic algorithm for engineering applications," *International Journal of Intelligent Engineering and Systems,* vol. 17, no. 5, pp. 1038-1047, 2024.

[31] F. A. Hashim, K. Hussain, E. H. Houssein, M. S. Mabrouk, and W. Al-Atabany, "Archimedes optimization algorithm: A new metaheuristic algorithm for solving optimization problems," *Applied Intelligence,* vol. 51, no. 3, pp. 1531-1551, 2021.

[32] I. Naidu, S. Srikanth, A. Rao, and A. Venkatanarayana, "A novel mine blast optimization algorithm (MBOA) based MPPT controlling for grid-PV systems," *AIMS Electronics & Electrical Engineering,* vol. 7, no. 2, pp. 145-160, 2023.

[33] V. Hayyolalam and A. A. P. Kazem, "Black widow optimization algorithm: A novel meta-heuristic approach for solving engineering optimization problems," *Engineering Applications of Artificial Intelligence,* vol. 87, p. 103249, 2020.

[34] J. S. Suri *et al.*, "UNet deep learning architecture for segmentation of vascular and non-vascular images: A microscopic look at UNet components buffered with pruning, explainable artificial intelligence, and bias," *Leee Access,* vol. 11, pp. 595-645, 2022.

[35] F. I. Diakogiannis, F. Waldner, P. Caccetta, and C. Wu, "ResUNet-a: A deep learning framework for semantic segmentation of remotely sensed data," *ISPRS Journal of Photogrammetry and Remote Sensing,* vol. 162, pp. 94-114, 2020.